



**HAL**  
open science

## New shear strength criteria for rock joints taking into account anisotropy of surface morphology

Tikou Belem, Françoise Homand, Mountaka Souley

► **To cite this version:**

Tikou Belem, Françoise Homand, Mountaka Souley. New shear strength criteria for rock joints taking into account anisotropy of surface morphology. 5. North American Rock Mechanics Symposium & 17. Tunneling Association of Canada Conference, Jul 2002, Toronto, Canada. pp.45-52. ineris-00972390

**HAL Id: ineris-00972390**

**<https://ineris.hal.science/ineris-00972390>**

Submitted on 3 Apr 2014

**HAL** is a multi-disciplinary open access archive for the deposit and dissemination of scientific research documents, whether they are published or not. The documents may come from teaching and research institutions in France or abroad, or from public or private research centers.

L'archive ouverte pluridisciplinaire **HAL**, est destinée au dépôt et à la diffusion de documents scientifiques de niveau recherche, publiés ou non, émanant des établissements d'enseignement et de recherche français ou étrangers, des laboratoires publics ou privés.

# New shear strength criteria for rock joints taking into account anisotropy of surface morphology

Tikou Belem

Department of Applied Sciences, University of Quebec in Abitibi-Temiscamingue, Rouyn-Noranda, PQ, Canada

Françoise Homand

LAEGO, Nancy School of Geology, Rue du Doyen M. Roubault, 54501 Vandoeuvre-les-Nancy Cedex, France

Mountaka Souley

INERIS, UMERG-LAEGO, Nancy School of Mine, Parc de Saurupt, 54042 Nancy Cedex, France

**ABSTRACT:** Three new peak shear stress criteria were proposed to predict the variation of shear strength with normal stress for dilatant (irregular and regular surfaces) and non-dilatant to slightly dilatant (planar rough surfaces or regularly undulated surfaces) rock joints under both constant normal stress (CNS) and constant normal stiffness (CNK) loading. The planar rough surfaces exhibit an isotropic nature whereas the undulated surfaces are anisotropic. These models take into account the progressive degradation of surface roughness during the course of monotonous or cyclic shearing. The third proposed model is a generalized new shear strength criterion which predict successfully the shear strength behavior of rock joints under CNS and CNK loading.

## 1. INTRODUCTION

The behavior of rock joints under either constant normal stress (CNS) or constant normal stiffness (CNK) loading conditions depends mainly on the wall surfaces roughness characteristics, the degree of matching and/or interlocking, the presence of filling materials and on the rock material properties. According to [1], the dominant factor influencing the mechanical behavior of rock joints is their morphology and roughness, and the most difficult thing is their characterization and modeling. The presence of discontinuities strongly affects the stability of rock engineering structures such as tunnels, underground mine excavations and open pits. The knowledge of the shear strength of rock joints is necessary when determining the stability of jointed rock masses. The variation of peak shear stress with normal stress has been modeled by many authors [2-7], and more recently by [8]. Although these models have substantially improved our knowledge on rock joints behavior, their limitations must be recognized [1]. In addition, few works have been devoted to take into account the progressive degradation of joint wall surface asperities during the course of monotonous or cyclic shearing [9-13].

The main purpose of the present study is to predict the peak shear stress of natural or artificial joints by taking into account the evolution of secondary and primary roughness through new proposed roughness parameters based on 3D laser profilometry [14, 15]. In the concept of primary and secondary asperities,

roughness is subdivided into two components: the secondary (or second-order) and the primary (or first-order) roughness [12,16,14]. The secondary asperities are defined by the surface heights distribution (which correspond to the *sensu stricto* roughness) while the primary asperities are defined by the overall geometry of the surface (which describe the surface anisotropy).

Based on joint initial morphological properties such as 2<sup>nd</sup> order asperities ( $DR_r$ ), surface angularity ( $\theta_s$ ), surface anisotropy/isotropy ( $k_a$ ), maximum asperity height ( $a_0$ ) and maximum shear displacement ( $u_s^{\max}$ ), two new shear strength ( $\tau_p$ ) criteria were proposed. This approach takes into account the matching/non matching and the dilatant/non dilatant nature of sheared joints. The strength behavior predicted by the proposed new shear strength criteria is compared to the results of some laboratory direct shear tests and to the shear strength criteria proposed by Ladanyi and Archambault [3], Saeb [7] and Barton [5].

## 2. NEW ROCK JOINT SURFACE ROUGHNESS PARAMETERS

In order to better characterize joint surface roughness which includes characteristics such as magnitude, angularity, undularity and anisotropy, numerous parameters have been proposed by Belem *et al.* [14] to supplement and overcome the inefficiency or the subjectivity of some of the already existing linear parameters (*e.g.*  $Z_z$ ,  $R_L$ ,  $P_s$  and  $JRC$ ). Some of these new parameters are

succinctly given below, but more details should be consulted in Belem *et al.* [14].

### 2.1. Profile mean angle, $\theta_p$

The profile mean angle was defined for describing its angularity. For a given joint topographic profile, the arithmetic mean angle of profile inclinations,  $\theta_p$ , is calculated along  $x$ - or  $y$ -axis by:

$$(\theta_p)_{k=x,y} = \tan^{-1} \left( \frac{1}{N_k - 1} \sum_{i=1}^{N_k-1} \left| \frac{z_{i+1} - z_i}{\Delta k} \right| \right) \quad (1)$$

where  $k$  denotes  $x$ - or  $y$ -axis;  $z_i$ , the discrete values of profile heights;  $(N_k-1)$ , the number of intervals used for slopes calculation along  $k$ -axis;  $\Delta k$ , the sampling step along  $k$ -axis (Fig. 1).

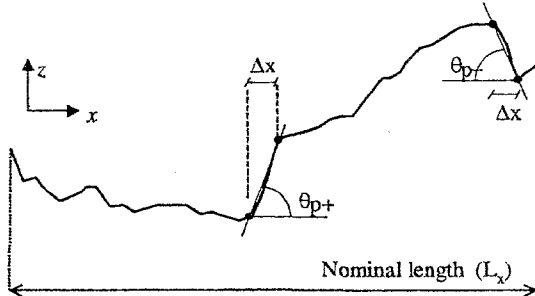


Fig. 1. Slopes and angles of a topographic profile along  $x$ -axis.

For the whole joint surface involving non-identical profile lengths (e.g. circular sections), the pseudo-surficial mean angle, defined as the weighted mean of the arithmetic mean profile angles in  $k$ -direction,  $(\bar{\theta}_p)_{k=x,y}$ , is given as follow:

$$(\bar{\theta}_p)_{k=x,y} = \text{atan} \left( \frac{\sum_{j=1}^{M_k} L_k^j \left( \frac{1}{N_k^j - 1} \sum_{i=1}^{N_k^j-1} \left| \frac{z_{i+1} - z_i}{\Delta k} \right| \right)}{\sum_{j=1}^{M_k} L_k^j} \right) \quad (2)$$

where  $M_k$  is the total number of profiles in  $k$ -direction ( $x$  or  $y$ );  $N_k^j$  the number of discrete points corresponding to the  $j^{\text{th}}$  profile along  $k$ -axis;  $L_k^j$  the length of the  $j^{\text{th}}$  profile along  $k$ -axis. When all the surface profiles have the same nominal length ( $L_k^j = L_k$ ; i.e. identical  $L_k^j$  in  $k$ -direction), Eq. (2) is reduced to an arithmetical mean.

### 2.2. Three-dimensional mean angle, $\theta_s$

By considering that the joint wall surface is made up of an assembly of elementary flat surfaces defined by topographical data ( $x, y, z$ ), the spatial orientation of each elementary surface is

characterized by the azimuth and the inclination angle,  $\theta$ , of its normal unit vector (Fig. 2).

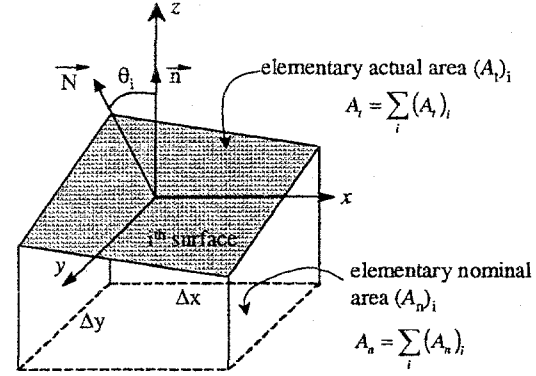


Fig. 2. The  $i^{\text{th}}$  elementary surface showing the angle  $\theta_i$ .

The three-dimensional mean angle is calculated from the angles  $\theta_i$  of normal vectors of all the elementary mean planes as follow:

$$\theta_s = \frac{1}{m} \sum_{i=1}^m \theta_i \quad (3)$$

where  $m$  is the total number of elementary surfaces. Angle  $\theta_s$  is considered as the mean angle of surface asperities or surface angularity.

### 2.3. Degree of surface apparent anisotropy, $k_a$

The pseudo-surficial mean angle calculated along both  $x$ - and  $y$ -directions,  $\bar{\theta}_p$ , can well describe the apparent structural anisotropy of surfaces in the  $xy$  plane. The degree of surface apparent anisotropy,  $k_a$ , is defined by the ratio of the anisotropy ellipse small half-axis  $b$  to its big half-axis  $a$  by the following relationships :

$$k_a = \frac{b}{a} = \frac{\min \{ (\bar{\theta}_p)_{x,y} \}}{\max \{ (\bar{\theta}_p)_{x,y} \}} \quad (0 \leq k_a \leq 1) \quad (4)$$

Subscript  $x$  or  $y$  denotes respectively the direction in which the individual profiles arithmetic mean angle,  $\theta_p$ , have been calculated. When  $0 \leq k_a < 0.25$ , surface is anisotropic (e.g.  $k_a = 0$  corresponds to surfaces with saw teeth, undulating surfaces, etc.); when  $0.25 \leq k_a < 0.5$ , surface is more anisotropic than isotropic; when  $0.5 \leq k_a < 0.75$ , surface is more isotropic than anisotropic; when  $0.75 \leq k_a \leq 1$ , surface is considered isotropic (e.g.  $k_a = 1$  corresponds to a perfectly isotropic surface).

### 2.4. Degree of surface roughness, $DR_r$

Joint surface roughness coefficient,  $R_s$ , has been defined for a single joint wall by El Soudani [17] as the ratio of the actual joint wall area,  $A_t$ , and the nominal surface area,  $A_n$  (see Fig. 2) as follow :

$$R_s = \frac{\sum_i (A_r)_i}{\sum_i (A_n)_i} = \frac{A_r}{A_n} \quad (1 \leq R_s \leq 2) \quad (5)$$

Actual surface area can be calculated either by surface triangulation or by integral method [14]. The upper limit value of  $R_s = 2$  was suggested by El Soudani [17] and is applicable to brittle fractures without recovering. The degree of joint surface roughness,  $DR_r$ , was defined from Eq. (5) in order to relate the evolution of surface roughness to its initial state by the following relationship:

$$DR_r = \frac{A_r - A_n}{A_r} = \frac{R_s - 1}{R_s} \quad (0 \leq DR_r < 1) \quad (6)$$

### 3. NEW SHEAR STRENGTH CRITERIA

Most of the existing shear strength criteria in the literature are developed to predict the peak shear stress of initially mated and interlocked joints displaying some dilatant behavior. If the majority of these models takes into account some aspects of joint initial roughness [3-7], very few models take into account the effect of both surface anisotropy [8] and progressive degradation of joint surfaces during the course of shearing [13]. In the present approach, authors suppose that there mainly exist two types of joint:

- (i.) non-dilatant joints (isotropic surfaces)
- (ii.) dilatant joints (isotropic/anisotropic surfaces)

We assume that dilatant joint surfaces (regular or irregular joints) are often anisotropic or more or less anisotropic where the primary roughness component plays a preponderant role. We also assume that non-dilatant joint surfaces (generally irregular) are more or less isotropic and where only the secondary roughness governs the shear strength behavior. In addition, we suppose that a dilatant joint will tend to be much less degraded than a non-dilatant joint which must be much degraded during the course of shearing. Dilatant joints are usually mated and/or interlocked while non-dilatant joints can be non-mated and non-interlocked (e.g. soil-structure, rock-structure, soil-rock, concrete-rock or mine backfill-rock interfaces).

Two shear strength criteria are proposed for the prediction of peak shear stress of non-dilatant joints exhibiting a strong potential of degradation and that of dilatant joints which exhibit a low potential of degradation. These criteria were formulated in the more general case of cyclic shearing where the shear stress-displacement curve ( $u_s, \tau$ ) is broken up into four portions (Fig. 3).

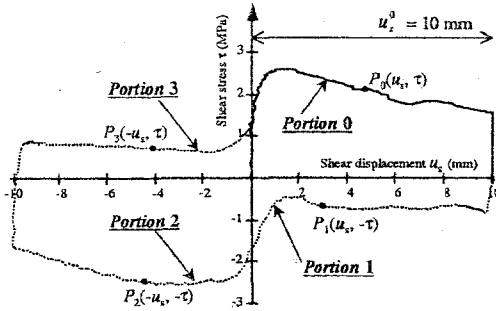


Fig. 3. Typical cyclic shear curve showing the four portions.

For each cycle of shearing the model will predict the peak shear stress ( $\tau_p$ ) on the first portion (Portion 0) of the ( $u_s, \tau$ ) curve as shown on Fig. 3. Shear displacement ( $u_s$ ) on the Portion 0 will be  $u_s^0$  and the shear displacement for one cycle of shearing will be of ( $4u_s^0$ ). With  $n$ , the number of cycles of shearing, the maximum cumulated shear displacement on the Portion 0,  $u_s^{\max} = u_s^0(4n - 3)$ . For a monotonous shearing,  $n = 1$  and  $u_s^{\max} = u_s^0$ . Another parameter to be taken into account in the formulation of the models is the maximum amplitude of surface heights,  $a_0$  (difference between maximum and minimum height of asperities), which is a constant.

#### 3.1. Shear strength criterion for non-dilatant joints

It was found from previous works [18] that the roughness of planar unmated and non-interlocked joints decreases a lot with the increase of normal stress and number of cycles of shearing (no significant dilatancy was observed). In addition, almost all the asperities have been sheared off after 5 cycles of shearing. It was concluded that the surface asperities degrade during the course of shearing by a progressive wear as well as by a collapse and leading to an increase in contact area and interfacial friction. Let  $\beta_n$  be the strength component in the shear behavior of rough, planar, almost isotropic and non-dilatant joint. The peak shear stress ( $\tau_p$ ) criterion for this type of joint which takes into account sliding through asperities and progressive degradation of asperities during the course of monotonous and cyclic shearing is given as follow :

$$\tau_p = \sigma_n \tan(\phi_r + \beta_n) \quad (7)$$

where  $\phi_r$  is the residual friction angle,  $\beta_n$  (subscript  $n$  denoting non-dilatant) is an angle describing the effect of joint roughness change due to asperities degradation. From our experimental investigations,

it was found that angle  $\beta_n$  is angle  $\theta_s$ -dependent and is given as follow:

$$\beta_n = \theta_s^0 (1 + w_n) \quad (8)$$

$$w_n = \frac{\sigma_n}{\sigma_c} \left[ \frac{a_0}{u_s^0} \times \frac{2k_a}{DR_r^0} \times \log \left( \frac{u_s^{\max}}{a_0} \right) \right] \quad (9a)$$

and in term of number of cycles of shearing :

$$w_n = \frac{\sigma_n}{\sigma_c} \left[ \frac{a_0}{u_s^0} \times \frac{2k_a}{DR_r^0} \times \log \left( \frac{u_s^0 (4n - 3)}{a_0} \right) \right] \quad (9b)$$

where  $\theta_s^0$  is the initial surface angularity;  $(1 + w_n)$  is the progressive degradation factor;  $\sigma_n$ , the normal stress;  $\sigma_c$ , the compressive strength of sample material;  $a_0$ , the maximum amplitude of surface;  $u_s^0$ , the shear displacement on the first portion (*Portion 0*) of shear curve (see Fig. 3);  $u_s^{\max}$ , the cumulated maximum shear displacement on the *Portion 0* (for  $n$  cycles of shearing,  $n > 0$ );  $k_a$ , the degree of surface apparent anisotropy;  $DR_r^0$ , the initial degree of surface roughness.

For unmated and non-interlocked rough planar joints, it was experimentally observed [14] that shear stress continuously increases with shear displacement and this means that angle  $\beta_n$  will increase with  $u_s^{\max}$  or the number of cycles  $n$ . Substituting Eqs. (8 & 9b) in Eq. (7), the new peak shear stress criterion for non-dilatant joints exhibiting a high potential of degradation is given as follow:

$$\tau_p = \sigma_n \tan \left( \phi_r + \theta_s^0 \left( 1 + \frac{\sigma_n}{\sigma_c} \left[ \frac{a_0}{u_s^0} \times \frac{2k_a}{DR_r^0} \times \log \left( \frac{u_s^{\max}}{a_0} \right) \right] \right) \right) \quad (10)$$

This peak shear stress criterion takes into account surface angularity ( $\theta_s$ ), surface anisotropy/isotropy ( $k_a$ ), strength of sample material ( $\sigma_c$ ), surface second-order roughness ( $DR_r^0$ ) and first-order roughness ( $a_0$ ) and finally, maximum cumulated shear displacement,  $u_s^{\max}$  (or number of cycles of shearing).

### 3.2. Shear strength criterion for dilatant joints

It was also found from previous investigations [13, 19] that for a moderately dilatant joint, cyclic shearing involved a progressive degradation of undulations which in turn increases contact areas and therefore the shear strength. Consequently, an efficient model must be able to take into account, the absence or the presence of pure dilatancy (sliding through asperities), the progressive degradation of asperities with shearing and the

friction of joint walls on debris. Among the numerous shear strength criteria for regular or irregular dilatant joints proposed by many authors, only those proposed by Ladanyi and Archambault [3], Jaegger [4], Barton [5] or Saeb [7] are more suitable to predict the shear strength of both regular and/or irregular joints. This is because these models take into account the change of initial roughness due to shearing. The common point between these different shear strength criteria is the significant contribution – even essential – of peak dilatancy angle ( $i_p$ ) in the formulation of these models. In this study we start from the Barton's criterion in which we replace the peak dilatancy angle ( $i_p$ ) by a new dilatancy-degradation angle which differs from  $i_p$ . According to Barton [5], the peak shear stress is related to peak dilatancy angle and joint initial roughness by the following equation:

$$\tau_p = \sigma_n \tan(\phi_b + i_p) \quad (11)$$

where  $\phi_b$  is the basic friction angle, and the peak dilatancy angle,  $i_p$ , is given by the relationship:

$$i_p = JRC \times \log \left( \frac{JCS}{\sigma_n} \right) \quad (12)$$

where JRC is the joint roughness coefficient; JCS the joint wall compressive strength.

In the first stage of this study authors attempted to reformulate Eq. (12) using the new previously proposed roughness parameters. It is well known from the numerous experimental studies in the literature and from our laboratory investigations that the peak dilatancy angle decreases non-linearly with the increase of normal stress. When comparing surface initial mean angle values,  $\theta_s^0$ , to those of experimental peak dilatancy angle,  $i_p$ , it was found that no trivial and simple relation does exist between these two angles. Experimental peak dilatancy angle is always greater than angle  $\theta_s^0$ , which was practically constant for the majority of samples. For a marked dilatant joint, the peak dilatancy angle was successfully predicted using an exponential model given by:

$$i_p = i_0 \exp \left( -A_1 \times \frac{\sigma_n}{\sigma_c} \right) \quad (13)$$

$$A_1 = \frac{10(k_a)^2}{DR_r^0} \quad (14)$$

where  $i_0$  represents the maximum inclination angle of surface prior to shearing (i.e. under  $\sigma_n = 0$ );  $A_1$  is a sample constant depending on the initial

roughness ( $DR_r^0$ ) and the degree of surface apparent anisotropy,  $k_a$ . From our investigations the maximum inclination angle,  $i_0$ , was estimated to be at least twice the 3D surface angle ( $i_0 = 2\theta_s^0$ ). Then, Eq. (13) become:

$$i_p = 2\theta_s^0 \exp\left(-\frac{10(k_a)^2}{DR_r^0} \times \frac{\sigma_n}{\sigma_c}\right) \quad (15)$$

Eq. (15) predicts well peak dilatancy angle for marked dilatant joints. But, substituting Eq. (15) in Barton's shear strength criterion (Eq. 11) leads to an underestimation of experimental peak shear stress. To better predict peak shear stress, a new angle must be defined in order to take into account both dilatancy phenomenon and degradation of surface asperities during the course of monotonous or cyclic shearing. This new dilatancy-degradation angle must be greater than the observed peak dilatancy angle ( $i_p$ ). Now, let  $i_d$  be this new angle (subscript  $d$  denotes dilatancy-degradation). Consequently, angle  $i_d$  will differs from the experimentally observed peak dilatancy angle ( $i_d > i_p$ ). Angle  $i_d$  describes the effect of dilatancy as well as the surface change due to asperities degradation which increases joint wall surface contact areas and hence the shear strength. Based on our experimental observations, angle  $i_d$  can be formulated as follows:

$$i_d = 2\theta_s^0 \exp\left(-A_2 \frac{\sigma_n}{\sigma_c}\right) \quad (16)$$

where  $A_2$  is a constant depending on initial roughness ( $DR_r^0$ ), degree of surface apparent anisotropy ( $k_a$ ), maximum amplitude of surface ( $a_0$ ) and maximum shear displacement,  $u_s^{\max}$  (or number of cycles,  $n$ ). It was found that constant  $A_2$  can be expressed as follows:

$$A_2 = \frac{u_s^0}{a_0} \left( \frac{u_s^0}{u_s^{\max}} + \left[ \frac{2(k_a)^2}{3 DR_r^0} \right] \right) \quad (17a)$$

and in term of number of cycles of shearing :

$$A_2 = \frac{u_s^0}{a_0} \left( \frac{1}{4n-3} + \left[ \frac{2(k_a)^2}{3 DR_r^0} \right] \right) \quad (17b)$$

and finally,

$$i_d = 2\theta_s^0 \exp\left(-\frac{\sigma_n}{\sigma_c} \times \frac{u_s^0}{a_0} \left[ \frac{u_s^0}{u_s^{\max}} + \frac{2(k_a)^2}{3 DR_r^0} \right] \right) \quad (18)$$

By substituting Eq. (18) in Eq. (11), the shear strength criterion for dilatant joints which includes the influence of dilatancy, asperities degradation

and the number of cycles of shearing is given as follow:

$$\tau_p = \sigma_n \tan\left(\phi_b + 2\theta_s^0 \exp\left(-\frac{\sigma_n}{\sigma_c} \times \frac{u_s^0}{a_0} \left[ \frac{u_s^0}{u_s^{\max}} + \left( \frac{2(k_a)^2}{3 DR_r^0} \right) \right] \right)\right) \quad (19)$$

### 3.3. Generalized shear strength criterion for dilatant joints

All the existing shear strength criteria are specifically formulated to predict the peak shear stress under constant normal shear stress (CNS) loading conditions. The main difference between CNS and CNK loading paths is that normal stiffness  $K_n = 0$  for CNS loading while  $K_n > 0$  for CNK loading. This is because  $\sigma_n > 0$  and is constant for CNS loading, while  $\sigma_n$  varies continuously during the course of shearing for CNK loading. Normal stiffness,  $K_n$ , is related to normal stress,  $\sigma_n$ , and normal displacement or dilatancy ( $u_n$ ) as follow:

$$K_n = \frac{d\sigma_n}{du_n} = \lim_{\Delta u_n \rightarrow 0} \frac{\Delta \sigma_n}{\Delta u_n} \quad (20a)$$

and

$$\begin{cases} \Delta \sigma_n = \sigma_n - \sigma_{ni} = K_n \Delta u_n \\ \sigma_n = \sigma_{ni} + K_n \Delta u_n \end{cases} \quad (20b)$$

where  $\sigma_{ni}$  is the initial normal stress.

Since we seek to predict the peak shear stress, then only the peak dilatancy ( $u_{np}$ ) will be considered ( $\Delta u_n \approx \Delta u_{np}$ ). Variation of peak dilatancy is related to dilatancy rate,  $\tan(i_{p\_CNK})$ , and incremental shear displacement,  $\Delta u_s$ , by the following relationship:

$$\Delta u_{np} = \Delta u_s \times \tan(i_{p\_CNK}) \quad (21)$$

As only the first portion (Portion 0) of the shear curve is considered (see Fig. 3) for the prediction of peak shear stress,  $\Delta u_s$  can reasonably be approximated by  $u_s^0$ , the shear displacement on the first portion ( $\Delta u_s \approx u_s^0$ ). Hence, Eq. (21) become:

$$\Delta u_{np} = u_s^0 \times \tan(i_{p\_CNK}) \quad (22)$$

Substituting Eq. (22) in Eq. (20b) leads to:

$$\sigma_{np} = \sigma_{ni} + K_n (u_s^0 \times \tan(i_{p\_CNK})) \quad (23)$$

where  $\sigma_{np}$  is the value of normal stress when the peak shear stress is reached during the course of CNK loading test.

From the proposed shear strength criterion for CNS loading path given by the relationship:

$$\tau_p|_{CNS} = \sigma_n \tan(\phi_b + i_d) \quad (24)$$

a generalized shear strength criterion can be derived for both CNS and CNK loading paths by substituting Eq. (23) in Eq. (24):

$$\tau_p|_{CNS,CNK} = \sigma_{np} \tan(\phi_b + i_d) \quad (25a)$$

$$\tau_p|_{CNS,CNK} = (\sigma_{ni} + K_n [u_s^0 \times \tan(i_p)]) \tan(\phi_b + i_d) \quad (25b)$$

and finally

$$\tau_p|_{CNS,CNK} = \sigma_{ni} \tan(\phi_b + i_d) + K_n (u_s^0 \times \tan(i_p)) \tan(\phi_b + i_d) \quad (26)$$

where  $i_p = i_{p,CNK}$

It was found from our experimental investigations that for a given  $\sigma_{ni}$ , peak dilatancy angle observed for the CNS loading ( $i_{p,CNS}$ ) is always greater than the peak dilatancy angle for the CNK loading ( $i_{p,CNK}$ ) due to the effect of the normal stiffness  $K_n$ . The CNK peak dilatancy angle can be predicted by the following relationship:

$$i_{p,CNK} = \theta_s^0 \exp\left(-\frac{(k_a)^2}{DR_r^0} \times \frac{K_n u_s^0}{\sigma_{ni} + \sigma_c}\right) \quad (27)$$

Eq. (27) is slight similar to Eq. (15) but different. In Eq. (26), the first term of the right hand side will correspond to the CNS loading condition when  $K_n = 0$ . If  $K_n > 0$ , Eq. (26) predicts the peak shear stress of CNK loading conditions.

#### 4. MONOTONOUS AND CYCLIC SHEAR TESTS

Monotonous and cyclic shear tests were carried out on three types of joint: a man-made regularly undulated mortar joint (Fig. 4a), a non-interlocked and non-mated granite joint with hammered surfaces (Fig. 4b), and a natural rough and undulated schist joint mortar replica (Fig. 4c).

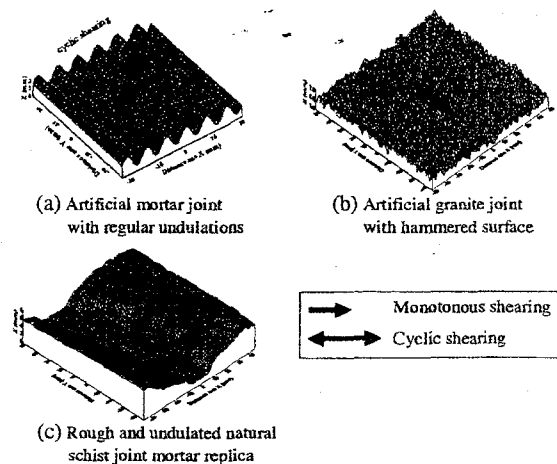


Fig. 4. Test samples. a) regular undulations b) hammered surface c) schist joint replica.

#### 4.1. Basic properties of test samples

The physical and mechanical properties of the test samples are listed in Tables 1.

Table 1. Test samples material properties

	Hammered joint surface	Rough and undulated	Regularly undulated
$\sigma_c$ (MPa)	152	75	75
$\sigma_t$ (MPa)	-10	-4	-4
$\phi_b$ (degree)	25	34	34

#### 4.2. Direct shear tests program

The hammered joints underwent 5 cycles of shearing, the man-made regularly undulated joints underwent 10 cycles of shearing and finally, the natural schist joint replicas underwent monotonous shearing under CNS loading conditions with  $\sigma_n$  ranging from 0.3–6 MPa. The CNK tests were carried out on the regularly undulated joint and the schist joint replica (Figs. 4a & c) under  $K_n$  ranging from 0.16–2 MPa/mm and  $\sigma_{ni}$  ranging from 0.4–2 MPa.

#### 4.3. Topography data acquisition

In order to estimate the morphological parameters of test samples, surfaces topography was measured prior to and after each shear test using a laser sensor profilometer. The roughness parameters calculated from these topographic data are listed in Table 2.

Table 2. Test samples initial morphological parameters

	$\theta_s$ (°)	$DR_r$	$k_a$	$a_0$ (mm)	$u_s^0$ (mm)	$u_s^{max}$ (mm)
Hammered	12.7	0.043	0.98	1.742	10	130
Undulated	10.3	0.023	0.21	2.000	10	370
Rough	11.9	0.045	0.43	8.703	20	20

#### 4.4. CNS test results

Tables 3–5 summarize the observed peak shear stress and peak dilatancy angle for the three types of test sample. The values are presented for the first cycle and the last cycle (5<sup>th</sup> cycle for the hammered joint and 10<sup>th</sup> cycle for the schist joint replica).

Table 3. Mechanical properties of hammered joint (Fig. 4b)

$\sigma_n$ (MPa)	$\tau_p$ (MPa)		$i_p$ (°)
	1 <sup>st</sup> cycle	5 <sup>th</sup> cycle	
0.3	0.220	0.251	-
1.2	1.009	1.149	-
4.0	3.003	3.613	-

Table 4. Mechanical properties of schist joint replica (Fig. 4c)

$\sigma_n$ (MPa)	$\tau_p$ (MPa)	$i_p$ (°)
0.4	0.637	19.70
0.8	1.147	15.50
1.2	1.665	12.62
1.8	2.356	9.20
2.4	2.872	7.03

Table 5. Mechanical properties of undulated joint (Fig. 4a)

$\sigma_n$ (MPa)	$\tau_p$ (MPa)		$i_p$ (°)	
	1 <sup>st</sup> cycle	10 <sup>th</sup> cycle	1 <sup>st</sup> cycle	10 <sup>th</sup> cycle
0.5	0.4	0.4	17	16
1.0	1.0	1.2	15	13
2.0	2.3	2.3	17	11
3.0	3.0	3.5	16	11
4.0	3.9	4.4	15	9.9
5.0	4.5	5.3	16	9.1
6.0	5.32	6.0	16	7.3

Fig. 5 shows the predicted peak shear stress by the new non-dilatant shear strength criterion (Eq. 10) for the hammered granite joint after the first and the last (5<sup>th</sup>) cycle of shearing and compared to experimental data. This figure shows that this new non-dilatant shear strength model is able to well predict the shear strength of non-dilatant or moderately dilatant joints. The peak shear strength predicted by the new dilatant shear strength model (Eq. 19) for the regularly undulated mortar joint and the schist joint replica are presented on Figs. 6 & 7. From these figures, good agreements between experiments and predictions is observed.

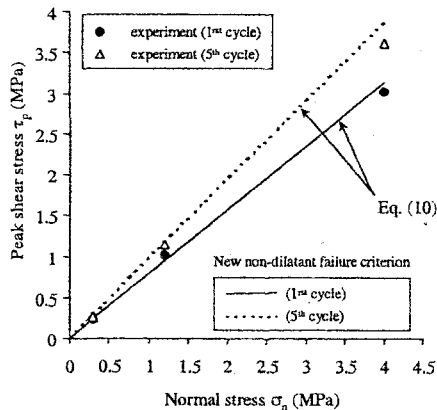


Fig. 5. Peak shear stress of the unmated hammered granite planar joint predicted by the new non-dilatant shear criterion.

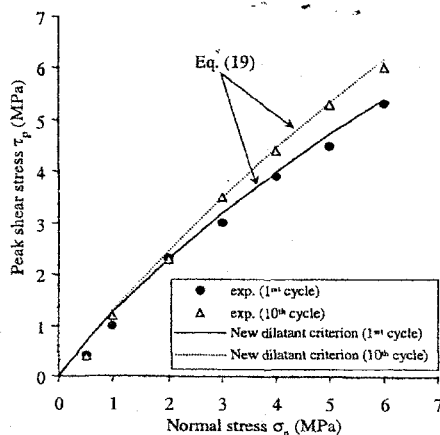


Fig. 6. Peak shear stress of the regularly undulated mortar joint predicted by the new dilatant shear criterion.

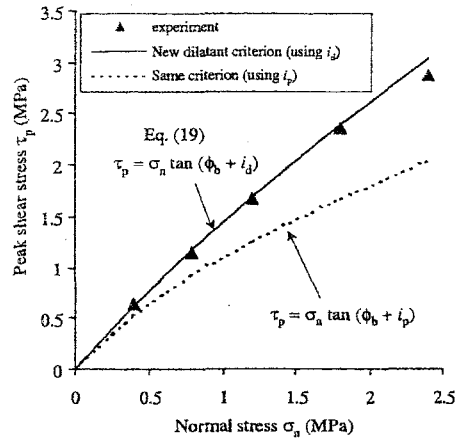


Fig. 7. Shear strength predicted by the new dilatant shear strength criterion when using dilatancy angle ( $i_p$ ) and the new proposed dilatancy-degradation angle ( $i_d$ ) and compared to the experimental results for the natural schist joint mortar replica.

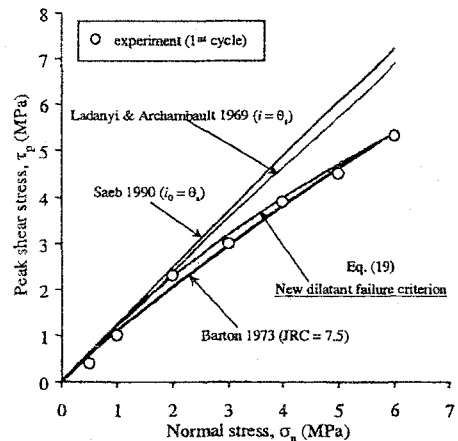


Fig. 8. Peak shear stress predicted with various shear strength criteria and compared to the new dilatant shear strength criterion for the regularly undulated joint.

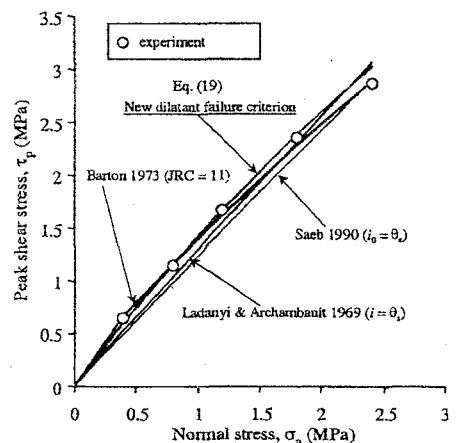


Fig. 9. Peak shear stress predicted with various shear strength criteria and compared to the new dilatant shear strength criterion for the natural schist joint mortar replica.

Figs. 8 & 9 shows the peak shear strength predicted by the new dilatant shear strength criterion (Eq. 19) for the undulated joint and the schist joint replica respectively. Examination of these figures shows that the proposed failure criterion and Barton's criterion are in good agreement with the experimental data.

#### 4.5. CNK test results

Tables 6 & 7 present the predicted CNK peak shear stress by the new proposed generalized shear strength criterion (Eq. 26). A good agreement is observed for the marked dilatant schist joint replica (Table 6) and for the moderately dilatant joint with regularly undulated surface (Table 7).

Table 6. Mechanical properties of schist joint replica (Fig. 4c)

$\sigma_{ni}$ (MPa)	$K_n$ (MPa/mm)	$i_{p,CNK}$ Eq. (27) (°)	$\tau_p$ exp. (MPa)	$\tau_p$ Eq. (26) (MPa)
0.4	0.16	10.42	1.40	1.54
0.4	1.00	5.17	3.10	3.94
0.8	0.32	9.13	2.35	2.49
1.2	0.48	8.01	2.15	2.84

Table 7. Mechanical properties of undulated joint (Fig. 4a)

$\sigma_{ni}$ (MPa)	$K_n$ (MPa/mm)	$i_{p,CNK}$ (°)	$\tau_p$ exp. (MPa)	$\tau_p$ Eq. (26) (MPa)
2.0	0.0	10.20	2.1	2.46
2.0	1.0	7.85	3.8	4.34
2.0	2.0	6.04	5.2	5.66

## 5. CONCLUSIONS

Based on new surface roughness parameters previously defined by authors [14], three new shear strength criteria were proposed to predict non-dilatant and dilatant shear strength behavior of rock joints. The first model (Eq. 10) was proposed for the prediction of the shear strength of unmated non-dilatant joints (isotropic surfaces). This shear strength model takes into account the progressive degradation of surface asperities. The second model was proposed to predict the shear strength of mated dilatant joints (anisotropic surfaces) under CNS loading. The third model is a generalized shear strength criterion for both CNS and CNK loading. These three models successfully predicted the shear strength of tested samples. Model parameters are the initial roughness and the shear displacement.

## REFERENCES

[1] Archambault, G., R. Flammang, J. Riss, and C. Sirieix. 1996. Joint shear behaviour revised on the basis of morphology 3D modelling and shear displacement. In *Rock Mech.*, Aubertin, Hassani&Mitri (eds), 1223-1230. Rotterdam : Balkema.

[2] Patton, F.D. 1966. Multiple modes of shear failure in rock. In *Proc. 1st. Congr. Int. Soc. Rock Mech.*, Lisbon, 509-513.

[3] Ladanyi, B. and G. Archambault. 1969. Simulation of the shear behaviour of a jointed rock mass. In *Proc. 11th Symp. on Rock Mech.*, Berkeley, 105-125.

[4] Jaegger, J.C. 1971. Friction of rocks and stability of rock slopes. *Geotechnique*, 21(2): 97-134.

[5] Barton, N.R. 1973. Review of a new shear strength criterion for rock joint deformation. *Engineering Geology*, 7: 287-332.

[6] Swan, G. and S. Zongqi. 1985. Prediction of shear behaviour of joints using profiles. *Rocks Mech. and Rocks Eng.* 18: 183-212.

[7] Saeb, S. 1990. A variance on Ladanyi and Archambault's shear strength criterion. In *Rock Joints*, Barton and Stephansson (eds), 701-705. Balkema, Rotterdam.

[8] Kulatilake, P.H.S.W., G. Shou, T.H. Huang, and R.M. Morgan. 1995. New peak shear strength criteria for anisotropic rock joints. *Int. J. Rock Mech. Min. Sci. and Geomech. Abstr.*, 32(7): 673-697.

[9] Plesha, M.E. 1987. Constitutive models for rock discontinuities with dilatancy and surface degradation. *Int. J. for Num. and Anal. Meth. in Geom.* 11: 345-362.

[10] Hutson, R.W., and C.H. Dowding. 1990. Joint asperity degradation during cyclic shear. *Int. J. Rock Mech. Min. Sci. & Geomech. Abstr.* 27(2): 109-119.

[11] Benjelloun, Z.H., M. Boulon, and D. Billiaux. 1990. Experimental and numerical investigation on rock joints. *Rock Joints*, Barton & Stephansson (eds), 171-178. Balkema Rotterdam.

[12] Jing, L., E. Nordlund, and O. Stephansson. 1993. Study of rock joints under cyclic loading conditions. *Rock Mech. Rock Engng.* 26(3): 215-232.

[13] Homand-Etienne, F., F. Lefèvre, T. Belem, and M. Souley. 1999. Rock joints behavior under cyclic direct shear tests. In *Proc. 37th U.S. Rock Mechanics Symp., June 6-9, 1999, Vail, Colorado*, Amadei, Kranz, Scott and Smealie (eds), 399-406.

[14] Belem, T., F. Homand, and M. Souley. 2000. Quantitative parameters for rock joint surface roughness. *Rock Mech. Rock Engng.* 33(4): 217-242.

[15] Belem, T., F. Homand-Etienne, and M. Souley. 1997. Fractal analysis of shear joint roughness. *Int. J. Rock Mech. & Min. Sci.* 34(3-4), paper No. 130.

[16] Kana, D.D., D.J. Fox, and S.M. Hsiung. 1996. Interlock/friction model for dynamic shear response in natural jointed rock. *Int. J. Rock Mech. Min. Sci. & Geomech. Abstr.* 33(4): 371-386.

[17] El Soudani, S.M. 1978. Profilometric analysis of fractures. *Metallography*, 11: 247-336.

[18] Belem, T. 1997. Morphology and mechanical behavior of rock discontinuities (in french). PhD thesis, INPL, Nancy, France : 220p.

[19] Lefèvre, F. 1999. Comportement mécanique et morphologique des discontinuités en cisaillement. Thèse de Doctorat INPL, Nancy, France : 144p.